Regular paper

Title

Identification and biochemical characterization of a heteromeric *cis*-prenyltransferase from the thermophilic archaeon *Archaeoglobus fulgidus*

Authors

Kitty Sompiyachoke, Arisa Nagasaka, Tomokazu Ito, and Hisashi Hemmi*

Affiliation

School of Agricultural Sciences and Graduate School of Bioagricultural Sciences, Nagoya University, Furo-cho, Chikusa-ku, Nagoya, Aichi 460-8601, Japan

Running title

Heterotetramer formation of archaeal *cis*-prenyltransferase

***Corresponding author**

Hisashi Hemmi

Phone: +81-52-789-4134 E-mail: hhemmi@agr.nagoya-u.ac.jp

Abbreviations

AfcPT, *Archaeoglobus fulgidus cis*-prenyltransferase; Bis-Tris, bis(2-hydroxyethyl)iminotris(hydroxymethyl)methane; CHAPS, 3-[(3-cholamidopropyl)dimethylammonio]-1-propanesulfonate; CHES, *N*-cyclohexyl-2-aminoethanesulfonic acid; cPT, *cis*-prenyltransferase; FPP, farnesyl pyrophosphate; IPP, isopentenyl pyrophosphate; MOPS, 3-morpholinopropanesulfonic acid; TAPS, [tris(hydroxymethyl)methylamino]propanesulfonic acid; TLC, thin-layer chromatography.

Abstract

cis-Prenyltransferases (cPTs) form linear polyprenyl pyrophosphates, the precursors of polyprenyl or dolichyl phosphates that are essential for cell function in all living organisms. Polyprenyl phosphate serves as a sugar-carrier for peptidoglycan cell wall synthesis in bacteria, a role which dolichyl phosphate performs analogously for protein glycosylation in eukaryotes and archaea. Bacterial cPTs are characterized by their homodimeric structure, while cPTs from eukaryotes usually require two distantly homologous subunits for enzymatic activity. This study identifies the subunits of heteromeric cPT, Af1219 and Af0707, from a thermophilic sulfur-reducing archaeon, *Archaeoglobus fulgidus*. Both subunits are indispensable for cPT activity, and their protein-protein interactions were demonstrated by a pulldown assay. Gel filtration chromatography and chemical cross-linking experiments suggest that Af1219 and Af0707 likely form a heterotetramer complex. Although this expected subunit composition agrees with a reported heterotetrameric structure of human hCIT/NgBR cPT complex, the similarity of the quaternary structures is likely a result of convergent evolution.

Keywords

cis-prenyltransferase; archaea; dolichol; isoprenoid; enzyme structure

Introduction

Polyprenyl groups, biosynthesized through the action of *cis*-prenyltransferases (cPTs), are utilized as carriers for sugars or oligosaccharides in the biosynthesis of peptidoglycan and the modification of proteins [1, 2]. cPTs catalyze the condensation of IPP onto an allylic prenyl pyrophosphate in a strictly *cis* configuration and produce a prenyl pyrophosphate with an extended hydrocarbon chain. The reaction is usually repeated and finally yields oligo- or polyprenyl pyrophosphates, forming relatively short C_{10} neryl pyorphosphate to $C_{>10,000}$ natural rubber. Bacterial undecaprenyl pyrophosphate synthase (UPPS) consecutively condenses eight units of IPP onto a farnesyl pyrophosphate (FPP) primer to give typically C_{55} undecaprenyl pyrophosphate, a precursor of the sugar carrier undecaprenyl phosphate that is indispensable in peptidoglycan cell wall synthesis. Eukaryotic cPTs are called dehydrodolichyl diphosphate synthases (DHDDS) as their products are later reduced at the α terminal isoprene unit to form dolichyl phosphate, which acts analogously to undecaprenyl phosphate as a glycosyl carrier in post-translational protein modification. cPTs were also found in archaea [3-6], demonstrating the conservation of cPTs throughout all three domains of life. The archaeal enzymes yield shorter products such as undecaprenyl pyrophosphate that are utilized for the biosynthesis of dolichols, which are generally shorter than those from eukaryotes and reduced also at non-α positions [7-11].

Structural studies on bacterial cPTs such as *Micrococcus luteus* UPPS (MlUPPS) [12] and *Escherichia coli* UPPS (EcUPPS) [13] demonstrated that they are, as far as can be ascertained, homodimeric enzymes. In contrast to bacterial cPTs, studies have shown that eukaryotic cPTs have accessory subunits. Both yeast Rer2 and human hCIT, which are identified as DHDDSs in those species, respectively, lack predicted transmembrane

regions but localize to the ER membrane [14], and additionally, over-expression of hCIT only moderately increases cPT activity in the cell [15]. Furthermore, a study using *Arabidopsis thaliana* found that a mutation in *LEW1*, a gene distantly related to its DHDDS gene (*CPT1*), caused impaired dolichol biosynthesis [16]. Nogo-B receptor (NgBR) in humans and its yeast homolog Nus1, both homologous to LEW1 from *A. thaliana*, were discovered to be necessary for cPT activity. These proteins called cPT-like (or cPTL) interact with the DHDDS from their respective organisms in a manner where both binding partners stabilize each other and significantly enhance cPT activity [17]. Missense mutations in either subunit (hCIT or NgBR) in humans results in congenital glycosylation diseases with symptoms that include retinitis pigmentosa [18], congenital scoliosis, severe neurological impairment, refractory epilepsy, and hearing deficit [19]. NgBR plays a multifaceted role in the cell, where in addition to being a component of the cPT machinery, it also serves as an integrated component in cholesterol trafficking and endothelial development [20] and has elevated mRNA expression in human cancers [21]. In recent years, an increasing number of NgBR homologs (or cPTL proteins) have been identified as being necessary for cPT activity, building evidence that eukaryotic cPTs have heteromeric structures, by pairs that include: CPT1 and CPTL1 in lettuce [22]; SlCPT3 and SlCPTBP in tomato [23]; SpRer2 and SpNus1 in *Schizosaccharomyces pombe* [19]; HRT1 and HRBP in para rubber tree [24]; and CPT1 and CPB in guayule [25]. Recently, structural studies of the hCIT/NgBR hetero-complex of human cPT were performed independently by two groups [26, 27], one of which reported a heterotetrameric structure formed by full-length hCIT and N-terminal truncated NgBR [26].

Our recent study demonstrated that two of three cPT homologs, MM_0618 and

MM_1083 from a methanogenic archaeon, *Methanosarcina mazei*, function in vitro as a cPT in a heteromeric manner where both subunits must be present for activity [3]. This data indicating the existence of heteromeric cPT in archaea raises new questions about the enzymes: Do eukaryotic and archaeal heteromeric cPTs have the same structural organization and perhaps ultimately– the same evolutionary origin? Unfortunately, the heteromeric cPT subunits from *M. mazei* were very unstable when isolated and unsuitable for further enzymological study. This situation motivated us to isolate cPT homologs from a thermophilic sulfate-reducing archaeon, *Archaeoglobus fulgidus*. These candidates are homologous to the cPT subunits from *M. mazei* and other heteromeric cPTs of eukaryotic origin: Af1219 is homologous to hCIT and MM_0618, and Af0707 is homologous to NgBR and MM_1083. In this study, Af1219 and Af0707 were recombinantly expressed in *E. coli* cells and purified independently, or together when expressed from a bicistronic vector, indicating the presence of protein-protein interaction between them. Radiometric assays showed that both subunits are required for cPT activity and the formation of polyprenyl pyrophosphates. The subunits and their heterocomplex were biochemically characterized, and clues about their quaternary structures were ascertained using gel filtration chromatography and through chemical cross-linking.

Results

Amino acid sequence alignment of cPT subunits

We searched the cPT homologs of *A. fulgidus* using the *M. mazei* cPT proteins MM_0014, MM_0618, and MM_1083 as queries and found that only two cPT homologs, Af0707 and Af1219, are encoded in the genome of *A. fulgidus*. Af0707 is highly homologous to MM1083 (43% sequence identity), which is related with eukaryotic cPTL proteins such as human NgBR as demonstrated in our previous study [3], while Af1219 is homologous to MM0618 (51% identity) and eukaryotic DHDDS such as hCIT. The amino acid sequences of the subunits of putative heteromeric cPT from *A. fulgidus* (AfcPT) were aligned against those of other cPTs, both homomeric and heteromeric in nature (Figure 1). The molecular masses of Af1219 and Af0707 are calculated to be 30.1 kDa and 24.3 kDa, respectively; therefore, we call Af1219 the "large" subunit and Af0707 the "small" subunit. Homomeric cPTs have been identified to harbor five conserved regions [1]. The heteromeric cPT "small" subunit group, which includes eukaryotic cPTL proteins although some cPTL proteins are larger than their partner cPT subunits, entirely lack region II and have low conservation of amino acid residues in regions I and III. On the other hand, regions IV and V form the dimer interface in *M. luteus* and *E. coli* UPPS enzymes (MlUPPS and EcUPPS) and are well conserved in all the aligned cPT sequences including both "small" and "large" subunits. Interestingly, all previously identified catalytic residues of UPPSs and DHDDSs are missing from the cPT small subunits. Within region I, Asp29 in MlUPPS and Asp26 in EcUPPS have been found to be situated within a p-loop [28], a motif frequently occurring in phosphate-binding proteins [29], which coordinates the necessary Mg^{2+} ion that is required for the binding of the S1 (allylic substrate-binding site) pyrophosphate.

Another set of strictly conserved residues, Ser71 and Asp74 in EcUPPS, are responsible for the proton relay required for the deprotonation of the C2 of IPP through a prenyltransfer reaction [30]. Lastly, a completely conserved pair of arginine residues (Arg194 and Arg200 in EcUPPS) bind to the S2 (IPP-binding site) pyrophosphate to coordinate substrate binding in the active site [30]. Importantly, though the cPT small subunits (or cPTL proteins) lack all these catalytic residues and were previously thought to only function as a docking protein [22], they share with homomeric enzymes a recently identified C-terminal RXG motif that is critical for enzymatic activity [31]. The arginine in the motif is replaced with an asparagine in many plants and fungal species [19] and by threonine in a homodimeric cPT from *M. mazei*, MM_0014 [32]. Interestingly, the RXG motif is missing from the large subunits of heteromeric cPTs. In the crystal structures of some bacterial homodimeric cPTs, the C-terminal extends into the catalytic site of the counter subunit and allows the conserved arginine in the RXG motif to interact with Mg^{2+}-coordinated water molecules, which probably stabilizes the enzyme-substrates-Mg^{2+} complex [32]. Mutation of the equivalent arginine residue in NgBR has been found to result in a drastic decrease in cPT activity, both in vitro and in vivo, and manifests pathologically as glycosylation defects [19]. Af1219 exhibits all the characteristics of a cPT large subunit: Asp29 exists to fulfill the role of Mg^{2+} binding, Ser74 and Asp77 form the proton shuttle, Arg201 and Arg207 are present to bind to the S2 pyrophosphate, and it completely lacks the C-terminal RXG motif. Accordingly, Af0707 largely resembles other cPT small subunits in which these residues are not conserved, yet the C-terminal RXG motif is present. Intriguingly, Af0707 probably lacks a transmembrane domain, which was reported to be present in the extended N-terminal of its eukaryotic counterparts such as human NgBR and *S. cerevisiae* Nus1.

These qualities in the primary sequences of the putative AfcPT subunits hint at their function as a heteromeric cPT, evoking further study.

Phylogenetic analysis of Af0707 and Af1219

A phylogenetic tree was constructed based on the protein sequence similarities of selected homomeric and heteromeric cPTs (Figure 2) from bacteria, archaea, and eukaryotes. The resultant tree is split into three clades: homodimeric cPTs from bacteria, large subunit proteins, and small subunit proteins of heteromeric cPTs. The archaeal cPT homologs in this study cluster with eukaryotic cPTs, suggesting that they share a common evolutionary origin and are likely to share structural and physiological functions. Indeed, dolichols formed from both eukaryotic and archaeal heteromeric cPTs are used in the same manner in post-translational protein modifications.

Heterocomplex formation for cPT activity

Af0707 or *Af1219* gene was introduced into a pET48b expression vector containing a thioredoxin-polyhistidine-tag-encoding sequence and a T7 promoter to construct plasmids for individual gene expression (Figure 3A). Both proteins were well-expressed and could be purified in high quantities through immobilized metal-ion affinity chromatography (Figure 3B). To determine if the complex formation is required for the activity, in vitro cPT activity assays were carried out using the independently purified proteins and ^{14}C-labeled IPP (Figure 3C). The assay involves measuring the level of radioactivity incorporated into the final cPT product mixture after allowing the reaction to proceed using FPP as the allylic primer. Both tagged-Af0707 and tagged-Af1219 on their own exhibit little or no cPT activity, while the mixture of both proteins

displayed high cPT activity, suggesting that the formation of a Af1219/Af0707 heterocomplex is required for the active cPT. This finding serves as the first heteromeric cPT to be identified from thermophilic archaea.

We then constructed bicistronic vectors encoding both subunits with only one subunit carrying the purification tag (Figure 3A). When tagged-Af0707 and untagged-Af1219 were expressed in the same cells, untagged-Af1219 (30.1 kDa) was co-purified through affinity chromatography alongside tagged-Af0707 (40.7 kDa) in a roughly 1:1 ratio (Fig. 3B). In contrast, when Af0707 lacking a tag was co-expressed with tagged-Af1219 (46.5 kDa), co-purification of a comparable amount of untagged-Af0707 (24.3 kDa) with that of tagged-Af1219 could not be observed, likely due to its low expression level. We incubated the co-purified untagged-Af1219/tagged-Af0707 complex (hereafter is referred to as co-expressed AfcPT) with FPP and ^{14}C-labeled IPP, and analyzed the butanol-extracted reaction products by reversed-phase thin-layer chromatography (TLC) after phosphatase treatment (Fig. 3D). The result of the TLC analysis demonstrated that co-expressed AfcPT mainly yields $C_{55\text{-}60}$ polyprenyl pyrophosphates, which is consistent with a previous report by Taguchi et al. demonstrating that *A. fulgidus* uses $C_{55\text{-}60}$ dolichyl (octahydro-dodecaprenyl and octahydro-undecaprenyl) phosphate for N-glycosylation [8]. This result suggests that AfcPT is responsible for the biosynthesis of dolichols in *A. fulgidus*.

Structural characterization of AfcPT

The quaternary structure of the co-expressed AfcPT was investigated using gel filtration chromatography (Figure 4A). The enzyme eluted in a monodispersed peak that corresponds to a molecular weight of 129 kDa (peak E11 in Figure 4A). SDS-PAGE

analysis of the eluted proteins in the peak indicated that the molar ratio of tagged-Af0707 and untagged-Af1219 was 1:1 (Figure 4B). A chemical cross-linking treatment using a primary amine-reactive cross linker, bis(sulfosuccinimidyl) suberate (BS^3), resulted in the formation of a fuzzy protein band on SDS-PAGE gel with the maximum molecular mass of 80-90 kDa. This value agrees well with cross-linked two molecules of tagged-Af0707 rather than with cross-linked untagged-Af1219/tagged-Af0707 or two molecules of untagged-Af1219 (Figure 4C). This means that at least two molecules of Af0707 are contained in the co-expressd AfcPT complex, which is composed of 1:1 ratio of Af0707 and Af1219. The calculated molecular weight of a heterotetrameric complex composed of two units of tagged-Af0707 and two units of untagged-Af1219 is 142 kDa, which is enough close to the estimated value of 129 kDa from gel-filtration chromatography. The $\alpha 2\beta 2$ heterotetrameric composition of AfcPT is similar to that of a structure reported recently for crystallized human cPT [26]. We discuss further considerations of this conclusion later in the paper.

We also performed the gel-filtration chromatography analyses of independently-expressed and purified subunits of AfcPT to know their quaternary structures (Figure S1). Affinity-purified tagged-Af1219 was presumed to form a homotetramer complex by itself, which resembles the expected composition of AfcPT. In contrast, tagged-Af0707 likely forms a dimer, which seems to be in a good agreement with the result from a study that showed C-terminal truncated yeast Nus1 (cPTL subunit) crystallizes in a homodimeric configuration [33].

Biochemical characterization of AfcPT

A pure co-expressed AfcPT solution could also be obtained through a two-step

process involving immobilized metal-ion affinity chromatography followed by ion-exchange chromatography (Figure 5A). This process avoids the drawbacks of gel filtration chromatography such as sample dilution and long run-time. This ion-exchange chromatography-purified sample was used for biochemical characterization of the AfcPT heterocomplex. In accord with its thermophilic origin, AfcPT has highest catalytic activity at elevated temperatures greater than 50°C, with an experimental optimum at 65°C (Figure 5B). Although *A. fulgidus* has been described as growing between 60 and 95°C with an optimum of 83°C [34], we did not test temperatures higher than 65°C because the enzyme started to aggregate. To examine the effect of the thioredoxin-polyhistidine-tag, which is not thermostable, we attempted to cleave the tag sequence using a protease, but failed perhaps due to steric hindrance of the quaternary structure. Therefore, for the purpose of this study, the reaction temperature of the AfcPT was set to 65°C. AfcPT functions over a broad pH range (Figure 5C), having good catalytic activity between pH 6 and 9, with an optimum pH of 8.8. This is in agreement with values established for the human heterocomplex, which also functions well within the same pH range and has a reported optimum of pH 8 [31]. Similar to other homo- and heteromeric cPTs, AfcPT requires Mg^{2+} for catalytic activity (Figure 5D). The absence of Mg^{2+} results in no activity, and AfcPT functions well across a wide range of Mg^{2+} concentration, from 1 mM to 50 mM, with an optimum around 1-2 mM. Excess Mg^{2+} ions may disturb ion pairs between amino acids in the protein structure by their electrostatic attraction to hard anionic groups such as carboxylate [35].

Having identified the ideal reaction conditions for AfcPT, steady-state kinetic parameters for FPP and IPP were determined (Figure 6). Kinetic parameters were measured by maintaining a constant IPP concentration (20 μM) against varying FPP

263 concentrations, or a constant FPP concentration (8 μM) against varying IPP
264 concentrations. The K_M values were 2.27 μM for IPP and 0.217 μM for FPP. A roughly
265 two-fold higher V_{max} value was obtained when the IPP concentration was kept constant
266 compared to when the FPP concentration was constant. This might come from the
267 inhibitory effect of FPP, which is visible in Figure 6A as a decrease in mean reaction
268 velocity at concentrations above 1 μM FPP. A similar phenomenon has been observed
269 with the human hCIT/NgBR complex [31]. The k_{cat} value of 0.0904 s^{-1} for the AfcPT
270 was hence calculated from the V_{max} achieved at 20 μM IPP and varying concentrations
271 of FPP. The K_M values for IPP and FPP are comparable with those of other cPTs, both
272 homomeric and heteromeric, showing a greater affinity for FPP than for IPP by an order
273 of magnitude. The k_{cat} for the AfcPT, however, is much lower than those of human cPT
274 and *E. coli* UPPS (0.58 [31] and 2.5 s^{-1} [36], respectively), but this may be a
275 consequence of carrying out the cPT reaction at a lower-than-optimal temperature for
276 the AfcPT.
277
278

Discussion

Our results suggest that AfcPT forms a heterotetramer, in which two large and two small subunits assemble. Interestingly, the mixture of the independently purified subunits gave an active enzyme, which is contrary to a previous observation with eukaryotic cPTs in which the subunits of heteromeric cPT must be co-expressed and assembled during translation in order to form an active enzyme [19]. This may be due to the approach used in the previous study, where proteins were expressed using in vitro translation instead of expression in host organisms. Another reason may be that the presence of the transmembrane region in the small subunits of eukaryotic cPTs, which could cause the rapid aggregation of the small subunits in the absence of their partner large subunits. Indeed, also in the present study, the independently expressed tagged-Af0707 (small subunit) tends to aggregate quickly after purification. The small subunit does not have an obvious transmembrane region and likely attaches peripherally to the membrane instead of penetrating it. We observed lower solubility of Af0707 despite the presence of a thioredoxin-polyhistidine fusion tag and use of a detergent 8 mM 3-[(3-cholamidopropyl)dimethylammonio]-1-propanesulfonate (CHAPS). Regardless, since peaks corresponding to monomeric subunits or complexes formed by each subunit were not observed in the gel-filtration study, the heteromeric complex formation is highly likely to contribute largely to the stabilization of AfcPT.

The molecular evolution of heteromeric complex-forming cPTs is also of our interest. Are eukaryotic heteromeric cPTs direct descendants of those from ancient archaea? The result of the phylogenetic analysis of functionally-characterized heteromeric and homomeric cPTs shown in Fig. 2 suggests that the large and small subunit of heteromeric cPTs independently form monophyletic branches. Unlike the

large subunits and homodimeric cPTs, however, the small subunits have highly diverged sequences. This is likely due to low evolutionary pressure to conserve catalytically important sequences besides the C-terminal RXG motif. The fact that AfcPT forms a heterotetrameric complex, which agrees with the recently reported heterotetrameric structure of human hCIT/NgBR complex (pdb#: 6Z1N) [26], suggests conservation of the quaternary structure among heteromeric cPTs and furthermore implies their shared ancestral origins. In human cPT, additional α-helices (αC1 and αC2) in the C-terminal of the large subunit (hCIT) were reported to play key roles in the interaction between two hCIT/NgBR heterodimers (Figure 7A and B). Such additional C-terminal structures are absent in AfcPT, shown by the predicted structure model of the Af1219/Af0707 heterodimer that we constructed using the crystal structure of human hCIT/NgBR as a reference (Fig. 7C). This result shows that, for AfcPT, heterotetramer assembly in a similar configuration as human cPT is impossible. Thus, this shared heterotetramer formation is unlikely inherited from their common ancestor, but probably a result of convergent evolution. Further structural analysis will be needed for concrete elucidation of the quaternary structure of AfcPT.

AfcPT may be a good model for the study of heteromeric cPTs, in lieu of eukaryotic enzymes. For example, this highly-stable archaeal enzyme may enable site-directed mutagenesis studies that would be helpful to identify the biochemical mechanisms of heteromeric cPTs, such as recognition and binding of the subunits to each other, membrane localization, catalysis of consecutive prenyltransfer reaction, and the release of highly hydrophobic products in a membrane. The elucidation of these mechanisms is the target of our future studies using AfcPT or its homologs in different archaea.

Methods

Materials

[1-^{14}C]IPP (55 Ci/mol) was purchased from GE Healthcare. FPP and IPP were donated by Dr. Chikara Ohto, Toyota Motor Corporation. $C_{55\text{-}60}$ polyprenol standards were donated by Prof. Tokuzo Nishino, Tohoku University. Plates for TLC were silica gel 60 RP-18 F_{254S} sheet sold by Merck. Except where otherwise stated, all reagents were of analytical grade and were sourced from Nacalai Tesque, Japan, Kanto Chemical Co. Inc., Japan, Sigma Aldrich, USA, Dojindo Molecular Technologies, Inc., Japan, and FUJIFILM Wako Pure Chemical, Japan.

Phylogenetic analysis of cPTs

Amino acid sequences of both homomeric and heteromeric cPTs were taken from the Kyoto Encyclopedia of Genes and Genomes (KEGG, https://www.genome.jp/kegg/) [37]. Alignment and subsequent phylogenetic tree construction was carried out using MEGA7 [38]. Alignment was carried out using CLUSTAL W and phylogenetic analysis was performed using the following parameters: Statistical method, maximum likelihood; No. of bootstrap replications, 1500; substitutions type, amino acid; model/method, Poisson model; rates among sites, gamma distributed (G); No. of discrete gamma categories, 2; gaps/missing data treatment, complete deletion; ML heuristic method, NearestNeighborInterchange (NNI); initial tree for ML, make initial tree automatically (Default - NJ/BioNJ); branch swap filter, none.

Amino acid sequence alignment for Figure 1 was performed using PRALINE multiple sequence alignment program (http://www.ibi.vu.nl/programs/pralinewww/)

[39] using the following parameters: exchange weights matrix, BLOSUM62; associated gap penalties, 15 open 1 extension; and the remaining settings left on default.

Recombinant expression of Af1219 and Af0707

The pET48b-T-Af1219-Af0707 plasmid was constructed by amplifying the *af0707* and *af1219* genes from *A. fulgidus* genomic DNA using KOD Plus polymerase (TOYOBO, Japan) and the following primers, in which restriction sites are underlined: for *af1219*, 5'-ACTGTGGTACCAGATGATATTTCACAAAATTTATG-3' and 5'-GTATGGAATTCTCACACCACCTCGTG-3'; for *af0707*, 5'-ACTGTGTCGACAAGAAGGAGATATAATGCTGCAAGCACCAAAG-3' and 5'-GTATGGCGGCCGCTCATCTTCCATACCTTCTTTCCC-3'. The amplicons and empty pET48b vector were digested using restriction enzymes (TOYOBO, Japan) and ligated sequentially into the Kpn I/EcoR I and Sal I/Not I sites for *af1219* and *af0707*, respectively, using Ligation High ver. 2 (TOYOBO). A pET48b-T-Af1219 vector was obtained during this process.

The pET48b-T-Af0707-Af1219 plasmid was constructed in a similar manner using pET48b-T-Af1219-Af0707 as a template for gene amplification using KOD -Plus- Neo polymerase (TOYOBO) and the following primers: for *af0707*, 5'-ACTGTGGTACCAGATGCTGCAAGCACCAAAG-3' and 5'-GTATGGAATTCTCATCTTCCATACCTTCTTTCCC-3'; for *af1219*, 5'-ACTGTGTCGACAAGAAGGAGATATAATGATATTTCACAAAATTTATGAGAACAAG-3' and 5'-GTATGGCGGCCGCTCACACCACCTCGTGACTC-3'. A pET48b-T-Af0707 vector was also obtained during this process.

The sequences of the genes introduced were analyzed using the above stated or

T7 promoter primers with BigDye Terminator v3.1 Cycle Sequencing Kit (Applied Biosystems, USA) in an Applied Biosystems 3500 Genetic Analyzer to confirm successful cloning. All the plasmids were constructed in *E. coli* XL10 Gold cells, then individually transformed into *E. coli* C41(DE3) cells for protein expression. Cells were cultured in Luria-Bertani broth containing 50 mg/L kanamycin (Tokyo Chemical Industry, Japan) at 37°C until log phase, after which IPTG was added to a final concentration of 0.5 mM, the temperature lowered to 22°C, and cultivation continued overnight. Cells were harvested by centrifugation and stored at -30°C.

Affinity purification of recombinant proteins

Cells containing the expression vectors were lysed in buffer A (50 mM Tris-HCl, pH 8.5, 0.1 M NaCl, 8 mM CHAPS, 1 mM $MgCl_2$) with 10 mM imidazole (Kishida Chemical) via sonication, and the supernatant after centrifugation was loaded onto a 1 mL HisTrap FF column (GE Healthcare, USA). The column was washed with buffer A containing 20 mM imidazole, then the tagged protein was eluted from the column using buffer A containing 200 mM imidazole. The peak fraction of the protein eluted from HisTrap FF was analyzed by SDS-PAGE using a 12% acrylamide gel.

Gel filtration chromatography of co-expressed AfcPT

For molecular weight determination, the affinity-purified proteins from the cells containing pET48b-T-Af0707-Af1219 (co-expressed AfcPT) was concentrated to 1 mL using Vivaspin Turbo 15 (10,000 MWCO) Ultrafiltration Units (Sartorius, Germany) before loading onto a Hiload 16/600 Superdex 200 pg gel filtration column (GE Healthcare). The gel filtration chromatography was run using buffer A at a flow

400 rate of 0.8 mL/min for a total of 140 minutes using an AKTA Pure 25 chromatography
401 system (GE Healthcare). Column eluate was collected in 5 mL fractions, and the
402 fractions at 60-65 mL elution volumes were pooled to be used as gel-filtration-purified
403 AfcPT. A calibration curve was obtained for the gel filtration column using Blue
404 Dextran 2000 (>2000 kDa), thyroglobulin (669 kDa), apoferritin (443 kDa), β-amylase
405 (200 kDa), alcohol dehydrogenase (150 kDa), albumin (66 kDa), carbonic anhydrase
406 (29 kDa), and potassium ferricyanide (0.3 kDa).
407 The procedures of gel-filtration chromatography of each AfcPT subunit were
408 described in Supplementary Information.
409
410 **Chemical cross-linking experiments**
411 The buffer of the gel-filtration-purified AfcPT solution was exchanged into 100
412 mM sodium phosphate buffer, pH8.8, containing 0.15 M NaCl and 8 mM CHAPS,
413 using Amicon Ultra-4 (10 kDa cutoff) centrifugal filters (Millipore, USA). The solution
414 was concentrated to 500 μL, and then BS^3 was added to the solution at a final
415 concentration of 5.8 mM. After reaction at room temperature for 30 min, a quenching
416 buffer containing 1 M Tris-HCl, pH7.5, and 8 mM CHAPS was added to a volume
417 wherein the concentration of Tris reached 38.5 mM. The result of cross-linking reaction
418 was analyzed by SDS-PAGE using a 10% gel.
419
420 **Ion exchange chromatography of co-expressed AfcPT**
421 The affinity-purified proteins from the cells containing pET48b-T-Af0707-
422 Af1219 were buffer exchanged into buffer B (20 mM Tris-HCl, pH 8.8, 8 mM CHAPS)
423 containing 0.1 M NaCl and then concentrated to 1 mL using Vivaspin Turbo 4

Ultrafiltration Units (Sartorius). This sample was then loaded onto a 1 mL HiTrap Q HP (GE Healthcare) column, and the column was washed with buffer B containing 0.1 M NaCl until UV-absorption of the eluent returned to the baseline. Ion exchange chromatography was then run using a linear gradient of 0.1–1.0 M NaCl in buffer B over 60 minutes at a flow rate of 1 mL/min. Eluate was collected in 2 mL fractions, and the peak fractions were used for biochemical characterization of AfcPT.

Radiometric activity assay

Standard reaction mixtures contained 1 μM FPP, 20 μM [^{14}C]IPP (55 Ci/mol), 2 mM $MgCl_2$, 100 mM *N*-cyclohexyl-2-aminoethanesulfonic acid (CHES)-NaOH buffer, pH 8.8, and an appropriate amount of the purified enzyme, in 100 μL. To analyze pH dependence, the same concentration of bis(2-hydroxyethyl)iminotris(hydroxymethyl)methane (Bis-Tris)-HCl buffer (pH5.8-6.9), 3-morpholinopropanesulfonic acid (MOPS)-NaOH buffer (pH6.9-7.8), [tris(hydroxymethyl)methylamino]propanesulfonic acid (TAPS)-NaOH buffer (pH8.3-8.8), or CHES-HCl buffer (pH8.8-10.0) was used for reaction. The reaction mixture was incubated for 1 hour at 65°C using an aluminum heat block (TAITEC, Japan) and terminated by rapid cooling in an ice-cooled aluminum block. Then 600 μL 1-butanol saturated with saline and 200 μL saturated NaCl were added to the mixture, mixed thoroughly, and centrifuged to separate the organic layer and the aqueous layer. Radioactivity in 300 μL of the organic layer was measured using a liquid scintillation counter (Hitachi-Aloka, Japan) to calculate specific activity. To analyze thermal stability of co-expressed AfcPT, the enzyme solution was heated for 30 min at various temperatures and then centrifuged to remove denatured proteins. The supernatant was

used for enzyme assay.

Measurement of kinetic parameters

The kinetic parameters for IPP were measured using 100 µL reaction mixtures containing 8 µM FPP, 100 mM CHES-NaOH, pH 8.8, 2 mM $MgCl_2$, 2.83 nM purified co-expressed AfcPT, and 1-100 µM [^{14}C]IPP (11-1.1 Ci/mol). The kinetic parameters for FPP were measured using 20 µM [^{14}C]IPP (2.8 Ci/mol) and 0.25-10 µM FPP instead. The reactions were carried out to determine the initial rate of AfcPT (within 10% substrate consumption for the total reaction time), and the products were extracted as described above. The initial velocity data were plotted using Michaelis-Menten regression in GraphPad Prism 8 (GraphPad Software, USA) to obtain K_M and V_{max} values. The k_{cat} values were calculated from the V_{max} value obtained with variable FPP and constant IPP concentrations.

Thin-layer chromatography

The cPT reaction was carried out, and the products were extracted as in the radiometric activity assay. The entire organic layer was added to a 2:1 mixture of methanol and 0.5 M sodium acetate buffer, pH 4.6, containing 2 mg acid phosphatase from potato (Sigma Aldrich), and the products were dephosphorylated overnight at 37°C [40]. The dephosphorylated cPT products were extracted and concentrated in *n*-pentane. Reversed-phase TLC was run using a 39:1 mixture of acetone and water as the mobile phase. Visualization of the TLC autoradiogram was carried out using a Typhoon FLA 9000 Imager (GE Healthcare).

Acknowledgements

This work was supported by JSPS KAKENHI Grant Numbers 17H05437, 19H04651, and 20H02899 for H.H.

We thank Tohru Yoshimura, Graduate School of Bioagricultural Sciences, Nagoya University, for helpful discussions.

References

1. Takahashi, S. & Koyama, T. (2006) Structure and function of *cis*-prenyl chain elongating enzymes, *Chem Rec.* **6**, 194-205.

2. Yamashita, S. & Takahashi, S. (2020) Molecular mechanisms of natural rubber biosynthesis, *Annu Rev Biochem.* **89**, 821-851.

3. Emi, K. I., Sompiyachoke, K., Okada, M. & Hemmi, H. (2019) A heteromeric *cis*-prenyltransferase is responsible for the biosynthesis of glycosyl carrier lipids in *Methanosarcina mazei*, *Biochem Biophys Res Commun.* **520**, 291-296.

4. Hemmi, H., Yamashita, S., Shimoyama, T., Nakayama, T. & Nishino, T. (2001) Cloning, expression, and characterization of *cis*-polyprenyl diphosphate synthase from the thermoacidophilic archaeon *Sulfolobus acidocaldarius*, *J Bacteriol.* **183**, 401-4.

5. Mori, T., Ogawa, T., Yoshimura, T. & Hemmi, H. (2013) Substrate specificity of undecaprenyl diphosphate synthase from the hyperthermophilic archaeon *Aeropyrum pernix*, *Biochem Bioph Res Co.* **436**, 230-234.

6. Yamada, Y., Fukuda, W., Hirooka, K., Hiromoto, T., Nakayama, J., Imanaka, T., Fukusaki, E. & Fujiwara, S. (2009) Efficient in vitro synthesis of *cis*-polyisoprenes using a thermostable *cis*-prenyltransferase from a hyperthermophilic archaeon *Thermococcus kodakaraensis*, *J Biotechnol.* **143**, 151-156.

7. Eichler, J. & Guan, Z. (2017) Lipid sugar carriers at the extremes: The phosphodolichols Archaea use in *N*-glycosylation, *Biochim Biophys Acta Mol Cell Biol Lipids.* **1862**, 589-599.

8. Taguchi, Y., Fujinami, D. & Kohda, D. (2016) Comparative analysis of archaeal lipid-linked oligosaccharides that serve as oligosaccharide donors for Asn glycosylation, *J Biol Chem.* **291**, 11042-54.

9. Chang, M. M., Imperiali, B., Eichler, J. & Guan, Z. Q. (2015) *N*-linked glycans are assembled on highly reduced dolichol phosphate carriers in the hyperthermophilic archaea *Pyrococcus furiosus*, *Plos One.* **10**: e0130482

10. Guan, Z. Q., Meyer, B. H., Albers, S. V. & Eichler, J. (2011) The thermoacidophilic archaeon *Sulfolobus acidocaldarius* contains an unsually short, highly reduced dolichyl phosphate, *BBA-Mol Cell Biol L.* **1811**, 607-616.

11. Guan, Z. Q., Naparstek, S., Kaminski, L., Konrad, Z. & Eichler, J. (2010) Distinct glycan-charged phosphodolichol carriers are required for the assembly of the pentasaccharide *N*-linked to the *Haloferax volcanii* S-layer glycoprotein, *Mol Microbiol.* **78**, 1294-1303.

12. Fujihashi, M., Zhang, Y. W., Higuchi, Y., Li, X. Y., Koyama, T. & Miki, K. (2001) Crystal structure of *cis*-prenyl chain elongating enzyme, undecaprenyl diphosphate synthase, *Proc Natl Acad Sci U S A.* **98**, 4337-4342.

13. Chang, S. Y., Ko, T. P., Liang, P. H. & Wang, A. H. J. (2003) Catalytic mechanism revealed by the crystal structure of undecaprenyl pyrophosphate synthase in complex with sulfate, magnesium, and triton, *J Biol Chem.* **278**, 29298-29307.
14. Sato, M., Sato, K., Nishikawa, S., Hirata, A., Kato, J. & Nakano, A. (1999) The yeast *RER2* gene, identified by endoplasmic reticulum protein localization mutations, encodes *cis*-prenyltransferase, a key enzyme in dolichol synthesis, *Mol Cell Biol.* **19**, 471-83.
15. Sato, M., Fujisaki, S., Sato, K., Nishimura, Y. & Nakano, A. (2001) Yeast Saccharomyces cerevisiae has two *cis*-prenyltransferases with different properties and localizations. Implication for their distinct physiological roles in dolichol synthesis, *Genes Cells.* **6**, 495-506.
16. Zhang, H. R., Ohyama, K., Boudet, J., Chen, Z. Z., Yang, J. L., Zhang, M., Muranaka, T., Maurel, C., Zhu, J. K. & Gong, Z. Z. (2008) Dolichol biosynthesis and its effects on the unfolded protein response and abiotic stress resistance in *Arabidopsis*, *Plant Cell.* **20**, 1879-1898.
17. Harrison, K. D., Park, E. J., Gao, N., Kuo, A., Rush, J. S., Waechter, C. J., Lehrman, M. A. & Sessa, W. C. (2011) Nogo-B receptor is necessary for cellular dolichol biosynthesis and protein *N*-glycosylation, *EMBO J.* **30**, 2490-500.
18. Zelinger, L., Banin, E., Obolensky, A., Mizrahi-Meissonnier, L., Beryozkin, A., Bandah-Rozenfeld, D., Frenkel, S., Ben-Yosef, T., Merin, S., Schwartz, S. B., Cideciyan, A. V., Jacobson, S. G. & Sharon, D. (2011) A missense mutation in DHDDS, encoding dehydrodolichyl diphosphate synthase, is associated with autosomal-recessive retinitis pigmentosa in Ashkenazi Jews, *Am J Hum Genet.* **88**, 207-215.
19. Park, E. J., Grabinska, K. A., Guan, Z. Q., Stranecky, V., Hartmannova, H., Hodanova, K., Baresova, V., Sovova, J., Jozsef, L., Ondruskova, N., Hansikova, H., Honzik, T., Zeman, J., Hulkova, H., Wen, R., Kmoch, S. & Sessa, W. C. (2014) Mutation of Nogo-B Receptor, a subunit of *cis*-prenyltransferase, causes a congenital disorder of glycosylation, *Cell Metab.* **20**, 448-457.
20. Park, E. J., Grabinska, K. A., Guan, Z. Q. & Sessa, W. C. (2016) NgBR is essential for endothelial cell glycosylation and vascular development, *EMBO Rep.* **17**, 167-177.
21. Pula, B., Olbromski, M., Owczarek, T., Ambicka, A., Witkiewicz, W., Ugorski, M., Rys, J., Zabel, M., Dziegiel, P. & Podhorska-Okolow, M. (2014) Nogo-B receptor expression correlates negatively with malignancy grade and Ki-67 antigen expression in invasive ductal breast carcinoma, *Anticancer Res.* **34**, 4819-4828.
22. Qu, Y., Chakrabarty, R., Iran, H. T., Kwon, E. J. G., Kwon, M., Nguyen, T. D. & Ro, D. K. (2015) A lettuce (*Lactuca sativa*) homolog of human Nogo-B receptor interacts with *cis*-prenyltransferase and is necessary for natural rubber biosynthesis, *J Biol Chem.* **290**, 1898-

552 1914.
553 23. Brasher, M. I., Surmacz, L., Leong, B., Pitcher, J., Swiezewska, E., Pichersky, E. &
554 Akhtar, T. A. (2015) A two-component enzyme complex is required for dolichol biosynthesis
555 in tomato, *Plant J.* **82**, 903-914.
556 24. Yamashita, S., Yamaguchi, H., Waki, T., Aoki, Y., Mizuno, M., Yanbe, F., Ishii, T.,
557 Funaki, A., Tozawa, Y., Miyagi-Inoue, Y., Fushihara, K., Nakayama, T. & Takahashi, S.
558 (2016) Identification and reconstitution of the rubber biosynthetic machinery on rubber
559 particles from *Hevea brasiliensis*, *eLife.* **5**.
560 25. Lakusta, A. M., Kwon, M., Kwon, E. J. G., Stonebloom, S., Scheller, H. V. & Ro, D. K.
561 (2019) Molecular studies of the protein complexes involving *cis*-prenyltransferase in
562 guayule (*Parthenium argentatum*), an alternative rubber-producing plant, *Front Plant Sci.*
563 **10**.
564 26. Bar-El, M. L., Vankova, P., Yeheskel, A., Simhaev, L., Engel, H., Man, P., Haitin, Y. &
565 Giladi, M. (2020) Structural basis of heterotetrameric assembly and disease mutations in
566 the human *cis*-prenyltransferase complex, *Nat Commun.* **11**.
567 27. Edani, B. H., Grabinska, K. A., Zhang, R., Park, E. J., Siciliano, B., Surmacz, L., Ha, Y.
568 & Sessa, W. C. (2020) Structural elucidation of the *cis*-prenyltransferase NgBR/DHDDS
569 complex reveals insights in regulation of protein glycosylation, *Proc Natl Acad Sci U S A.*
570 **117**, 20794-20802.
571 28. Liang, P. H., Ko, T. P. & Wang, A. H. (2002) Structure, mechanism and function of
572 prenyltransferases, *Eur J Biochem.* **269**, 3339-54.
573 29. Kinoshita, K., Sadanami, K., Kidera, A. & Go, N. (1999) Structural motif of phosphate-
574 binding site common to various protein superfamilies: all-against-all structural comparison
575 of protein-mononucleotide complexes, *Protein Engineering.* **12**, 11-14.
576 30. Guo, R. T., Ko, T. P., Chen, A. P. C., Kuo, C. J., Wang, A. H. J. & Liang, P. H. (2005)
577 Crystal structures of undecaprenyl pyrophosphate synthase in complex with magnesium,
578 isopentenyl pyrophosphate, and farnesyl thiopyrophosphate - Roles of the metal ion and
579 conserved residues in catalysis, *J Biol Chem.* **280**, 20762-20774.
580 31. Grabinska, K. A., Edani, B. H., Park, E. J., Kraehling, J. R. & Sessa, W. C. (2017) A
581 conserved C-terminal RXG motif in the NgBR subunit of *cis*-prenyltransferase is critical for
582 prenyltransferase activity, *J Biol Chem.* **292**, 17351-17361.
583 32. Okada, M., Unno, H., Emi, K. I., Matsumoto, M. & Hemmi, H. (2021) A versatile *cis*-
584 prenyltransferase from *Methanosarcina mazei* catalyzes both *C*- and *O*-prenylations, *J Biol*
585 *Chem.* **296**.
586 33. Ma, J., Ko, T. P., Yu, X., Zhang, L., Ma, L., Zhai, C., Guo, R. T., Liu, W., Li, H. & Chen,
587 C. C. (2019) Structural insights to heterodimeric *cis*-prenyltransferases through yeast

588 dehydrodolichyl diphosphate synthase subunit Nus1, *Biochem Biophys Res Commun.* **515**,
589 621-626.
590 34. Stetter, K. O. (1988) *Archaeoglobus fulgidus* gen. nov., sp. nov.: a new taxon of
591 extremely thermophilic archaebacteria, *Systematic and Applied Microbiology.* **10**, 172-173.
592 35. Zeng, J., Gao, X. W., Dai, Z., Tang, B. & Tang, X. F. (2014) Effects of metal ions on
593 stability and activity of hyperthermophilic pyrolysin and further stabilization of this
594 enzyme by modification of a Ca^{2+}-binding site, *Appl Environ Microbiol.* **80**, 2763-2772.
595 36. Pan, J. J., Yang, L. W. & Liang, P. H. (2000) Effect of site-directed mutagenesis of the
596 conserved aspartate and glutamate on *E. coli* undecaprenyl pyrophosphate synthase
597 catalysis, *Biochemistry.* **39**, 13856-61.
598 37. Kanehisa, M. & Goto, S. (2000) KEGG: Kyoto encyclopedia of genes and genomes, *Nucl*
599 *Acids Res.* **28**, 27-30.
600 38. Kumar, S., Stecher, G. & Tamura, K. (2016) MEGA7: Molecular evolutionary genetics
601 analysis version 7.0 for bigger datasets, *Mol Biol Evol.* **33**, 1870-1874.
602 39. Simossis, V. A. & Heringa, J. (2005) PRALINE: a multiple sequence alignment toolbox
603 that integrates homology-extended and secondary structure information, *Nucl Acids Res.*
604 **33**, W289-W294.
605 40. Fujii, H., Koyama, T. & Ogura, K. (1982) Efficient enzymatic hydrolysis of polyprenyl
606 pyrophosphates, *Biochim Biophys Acta.* **712**, 716-8.
607 41. Waterhouse, A., Bertoni, M., Bienert, S., Studer, G., Tauriello, G., Gumienny, R., Heer,
608 F. T., de Beer, T. A. P., Rempfer, C., Bordoli, L., Lepore, R. & Schwede, T. (2018) SWISS-
609 MODEL: homology modelling of protein structures and complexes, *Nucl Acids Res.* **46**,
610 W296-W303.
611

612 **Figure legends**

613

614 **Figure 1.** Multiple sequence alignment of cPTs. Amino acid sequences were aligned
615 using PRALINE multiple sequence alignment program
616 (http://www.ibi.vu.nl/programs/pralinewww/) [39]. EcUPPS and MlUPPS: UPPS
617 (bacterial homodimeric cPT) from *E. coli* and *M. luteus*, respectively. Af1219,
618 MM_0618, hCIT, and Rer2: the large subunit of heteromeric cPT from *A. fulgidus*, *M.*
619 *mazei*, human and *S. cerevisiae*, respectively. Af0707, MM_1083, NgBR and Nus1: the
620 small subunit of heteromeric cPT from *A. fulgidus*, *M. mazei*, human and *S. cerevisiae*,
621 respectively. Stars represent catalytically important residues discussed in the main text.

622

623 **Figure 2.** Phylogenetic analysis of both homomeric and heteromeric cPT subunits.
624 Numbers represent bootstrap percentages from 1,500 replicates. EcUPPS, *E. coli* UPPS;
625 MlUPPS, *M. luteus* UPPS; hCIT and NgBR, the large and small subunits of human cPT,
626 respectively; ScRer2 and ScNus1, the large and small subunits of *S. cerevisiae* cPT,
627 respectively; Af1219 and Af0707, the large and small subunits of AfcPT, respectively;
628 MM0618 and MM1083, the large and small subunits of *M. mazei* cPT, respectively;
629 MA3723 and MA4402, the large and small subunits of *M. acetivorans* cPT,
630 respectively.

631

632 **Figure 3.** Confirmation of hetero-complex formation using recombinantly-expressed
633 AfcPT subunit proteins. (A) Vectors created for expression of individual tagged subunits
634 as well as co-expression of both subunits. T7, T7 promoter; Tag, the DNA sequence
635 encoding a thioredoxin-polyhistidine-tag; RBS, a ribosome binding-site sequence

636 located between tandemly placed genes. (B) SDS-PAGE analysis of AfcPT subunits
637 purified through affinity chromatography. M; molecular marker; lane 1, tagged-Af0707
638 purified from *E. coli* cells harboring pET48b-T-Af0707; lane 2: tagged-Af1219 purified
639 from cells harboring pET48b-T-Af1219; lane 3, co-expressed tagged-Af0707 and
640 untagged-Af1219 that were co-purified from cells harboring pET48b-T-Af0707-
641 Af1219; lane 4, tagged-Af1219 purified from cells harboring pET48b-T-Af1219-
642 Af0707. In lane 4, the protein band of untagged-Af0707 is unobservable. (C) Catalytic
643 activity of each AfcPT subunit or their mixture. The cPT activity of 0.5 μg of tagged-
644 Af0707, tagged-Af1219, or the mixture of both proteins (0.25 μg each) was measured in
645 triplicate. 0707, tagged-Af0707; 1219, tagged-Af1219. (D) Reverse-phased TLC
646 analysis of the products of co-expressed AfcPT after phosphatase treatment. $C_{55\text{-}60}$
647 polyprenols were used as authentic standards. s.f., solvent front; ori., origin.
648
649 **Figure 4.** Quaternary structure analyses of co-expressed AfcPT. (A) Chromatogram of
650 gel filtration chromatography of affinity-purified proteins. An arrowhead indicates the
651 peak of tagged-Af0707/untagged-Af1219 in multimeric assembly. E6, E11, E13, and
652 E16 represent the fractions containing major UV peaks at 280 nm. Inset: Calibration
653 curve for molecular weight determination of proteins. (B) SDS-PAGE analysis of the
654 peak fractions in (A). (C) SDS-PAGE analysis of AfcPT after chemical cross-linking
655 reaction with BS^3. Lane 1, gel-filtration-purified AfcPT without cross-linking; lane 2,
656 cross-linked AfcPT. An arrowhead represents a protein band of 80-90 kDa that has
657 newly emerged from cross-linking.
658
659 **Figure 5.** Investigation of biochemical characteristics of the AfcPT heterocomplex. (A)

660 SDS-PAGE analysis of AfcPT purified through affinity chromatography and ion-
661 exchange chromatography. Lane 1: flow-through fraction of the ion-exchange
662 chromatography; lane 2: purified AfcPT. (B) Temperature dependency of AfcPT
663 activity. (C) pH specificity of AfcPT. Buffer systems used were: 100 mM Bis-Tris-HCl
664 (pH5.8-6.9), 100 mM MOPS-NaOH (pH6.9-7.8), 100 mM TAPS-NaOH (pH8.3-8.8),
665 and 100 mM CHES-NaOH (pH8.8-10.0). (D) Magnesium ion dependency of AfcPT
666 activity.
667
668 **Figure 6.** Determination of kinetic parameters of AfcPT for FPP (A) and IPP (B). As the
669 companion substrate for the cPT reaction, 20 μM IPP and 8 μM FPP were used in (A)
670 and (B), respectively. Each data point is a mean of three individual trials.
671
672 **Figure 7.** Comparison of the crystal structure of human cPT and the model structure of
673 AfcPT. (A) Crystal structure of human cPT in a hCIT/NgBR heterodimeric complex
674 form (PDB ID: 6W2L). This structure was selected as the most suitable template and
675 used for AfcPT modeling. hCIT and NgBR subunits are colored in green and cyan,
676 respectively. Additional N-terminal α-helices in hCIT are colored in pale green. (B)
677 Heterotetrameric structure reported for human cPT (PDB ID: 6Z1N). The additional α-
678 helices of the large subunits (hCIT, green and orange) are represented by paler colors.
679 (C) Model structure of AfcPT in a Af1219/Af0707 heterodimeric complex form.
680 Homology modeling was performed using the SWISS-MODEL web service
681 (https://swissmodel.expasy.org) [41] with default conditions. Af1219 and Af0707
682 subunits are colored in green and cyan, respectively.

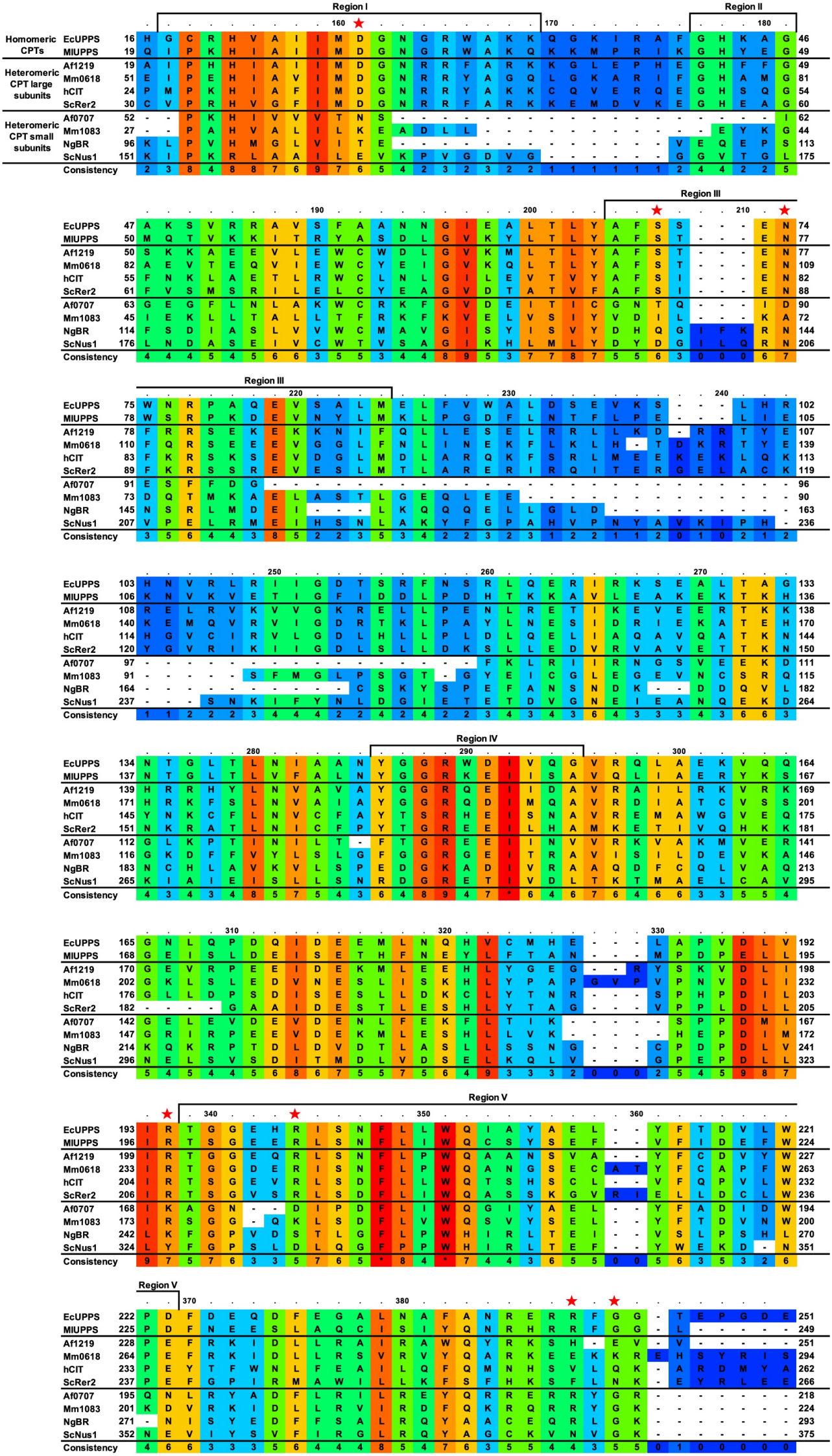
Region I
Region II
Region III
Region IV
Region V
Homomeric CPTs
Heteromeric CPT large subunits
Heteromeric CPT small subunits
EcUPPS
MtUPPS
Af1219
Mm0618
hCIT
ScRer2
Af0707
Mm1083
NgBR
ScNus1
Consistency

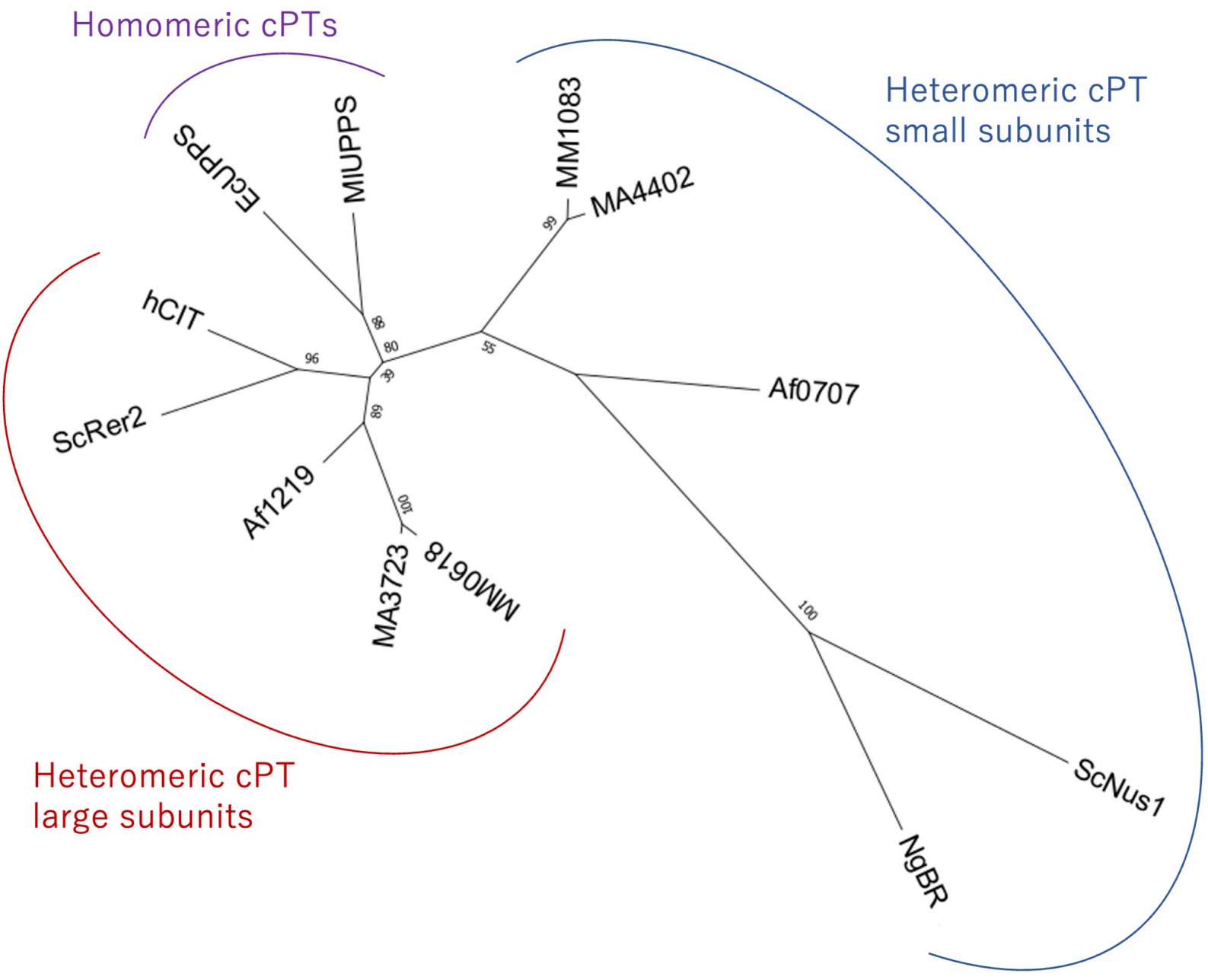
Homomeric cPTs
Heteromeric cPT
small subunits
Heteromeric cPT
large subunits
EcUPPS
MlUPPS
MM1083
MA4402
hCIT
ScRer2
Af1219
MA3723
MM0618
Af0707
ScNus1
NgBR
88
80
96
66
55
89
100
99
100

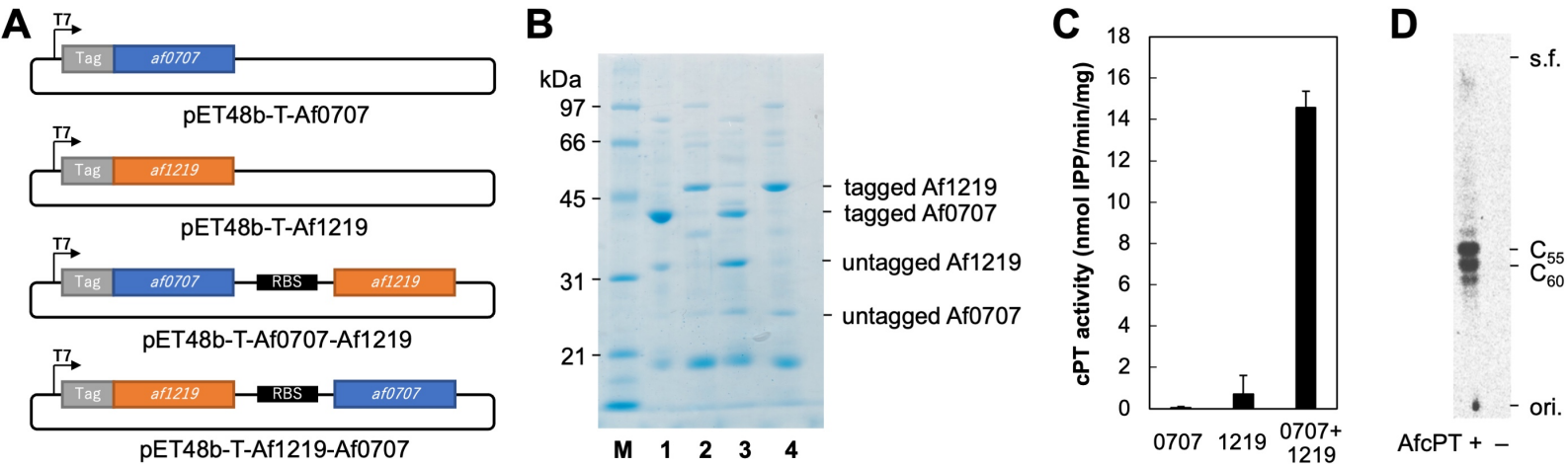
A
T7
Tag
af0707
pET48b-T-Af0707
T7
Tag
af1219
pET48b-T-Af1219
T7
Tag
af0707
RBS
af1219
pET48b-T-Af0707-Af1219
T7
Tag
af1219
RBS
af0707
pET48b-T-Af1219-Af0707
B
kDa
97
66
45
31
21
M
1
2
3
4
tagged Af1219
tagged Af0707
untagged Af1219
untagged Af0707
C
cPT activity (nmol IPP/min/mg)
18
16
14
12
10
8
6
4
2
0
0707
1219
0707+
1219
D
s.f.
C55
C60
ori.
AfcPT + –

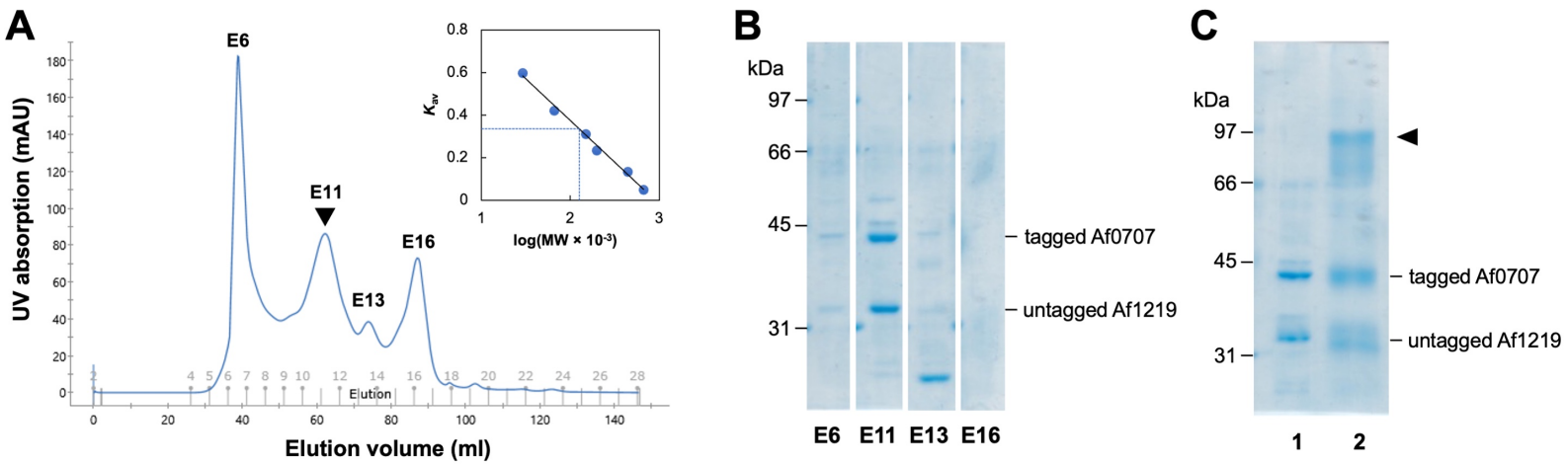
A
E6
E11
E13
E16
UV absorption (mAU)
Elution volume (ml)
Elution
K_{av}
log(MW × 10^{-3})
B
kDa
97
66
45
31
tagged Af0707
untagged Af1219
E6
E11
E13
E16
C
kDa
97
66
45
31
tagged Af0707
untagged Af1219
1
2

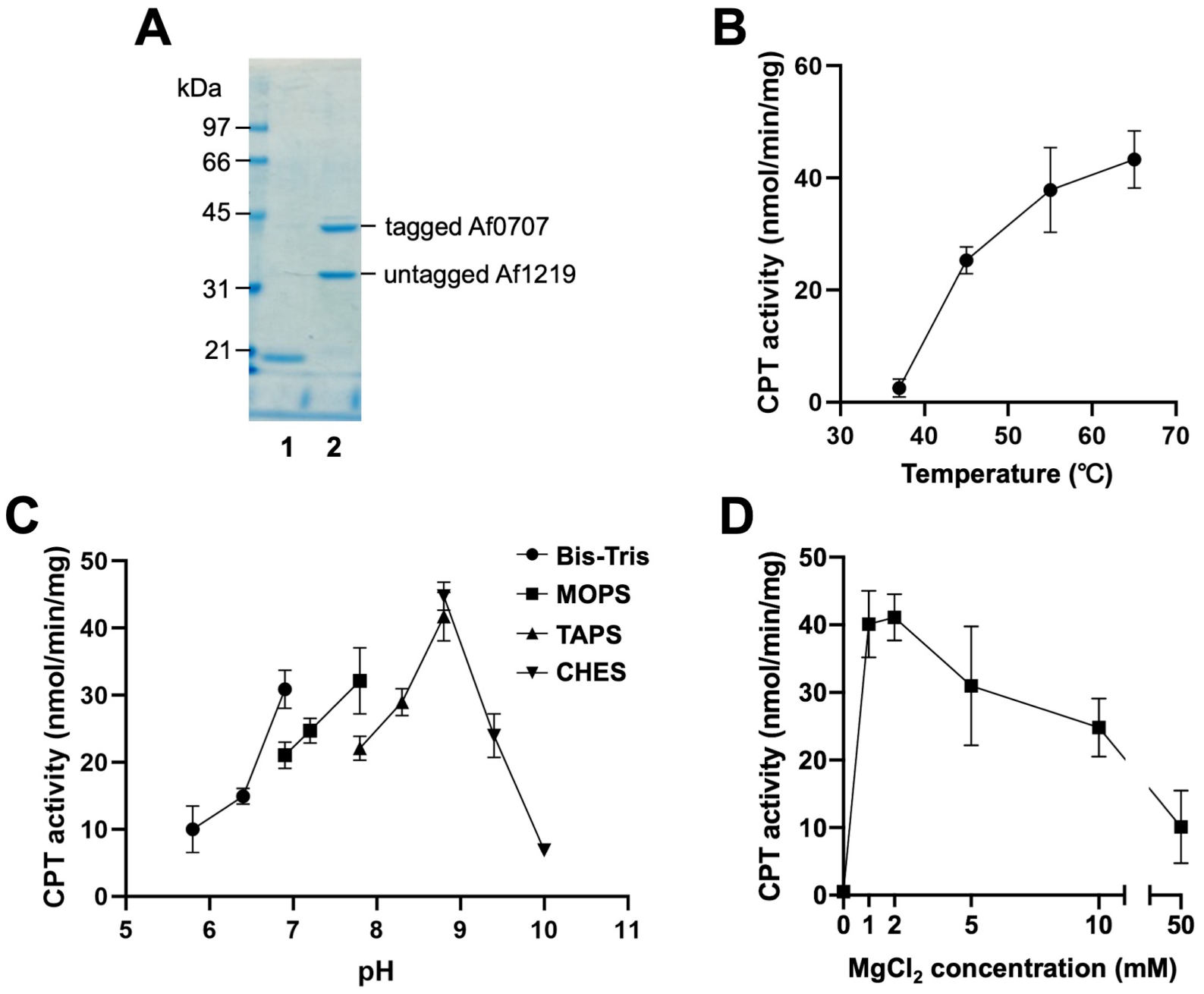
A
kDa
97
66
45
31
21
tagged Af0707
untagged Af1219
1
2
B
CPT activity (nmol/min/mg)
60
40
20
0
30
40
50
60
70
Temperature (℃)
C
CPT activity (nmol/min/mg)
50
40
30
20
10
0
5
6
7
8
9
10
11
pH
Bis-Tris
MOPS
TAPS
CHES
D
CPT activity (nmol/min/mg)
50
40
30
20
10
0
0
1
2
5
10
50
MgCl2 concentration (mM)

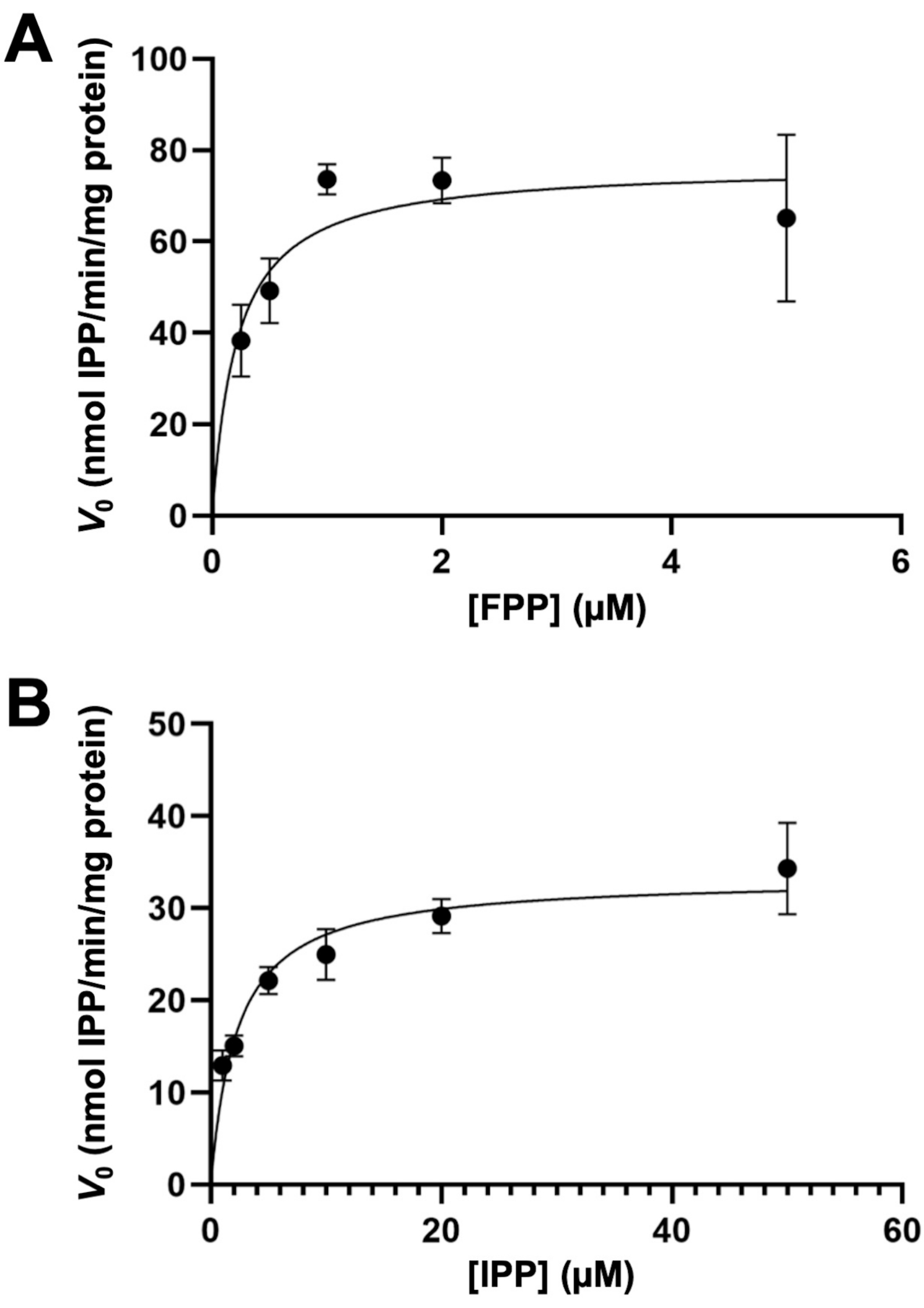
A
100
80
60
40
20
0
V_0 (nmol IPP/min/mg protein)
0
2
4
6
[FPP] (μM)
B
50
40
30
20
10
0
V_0 (nmol IPP/min/mg protein)
0
20
40
60
[IPP] (μM)

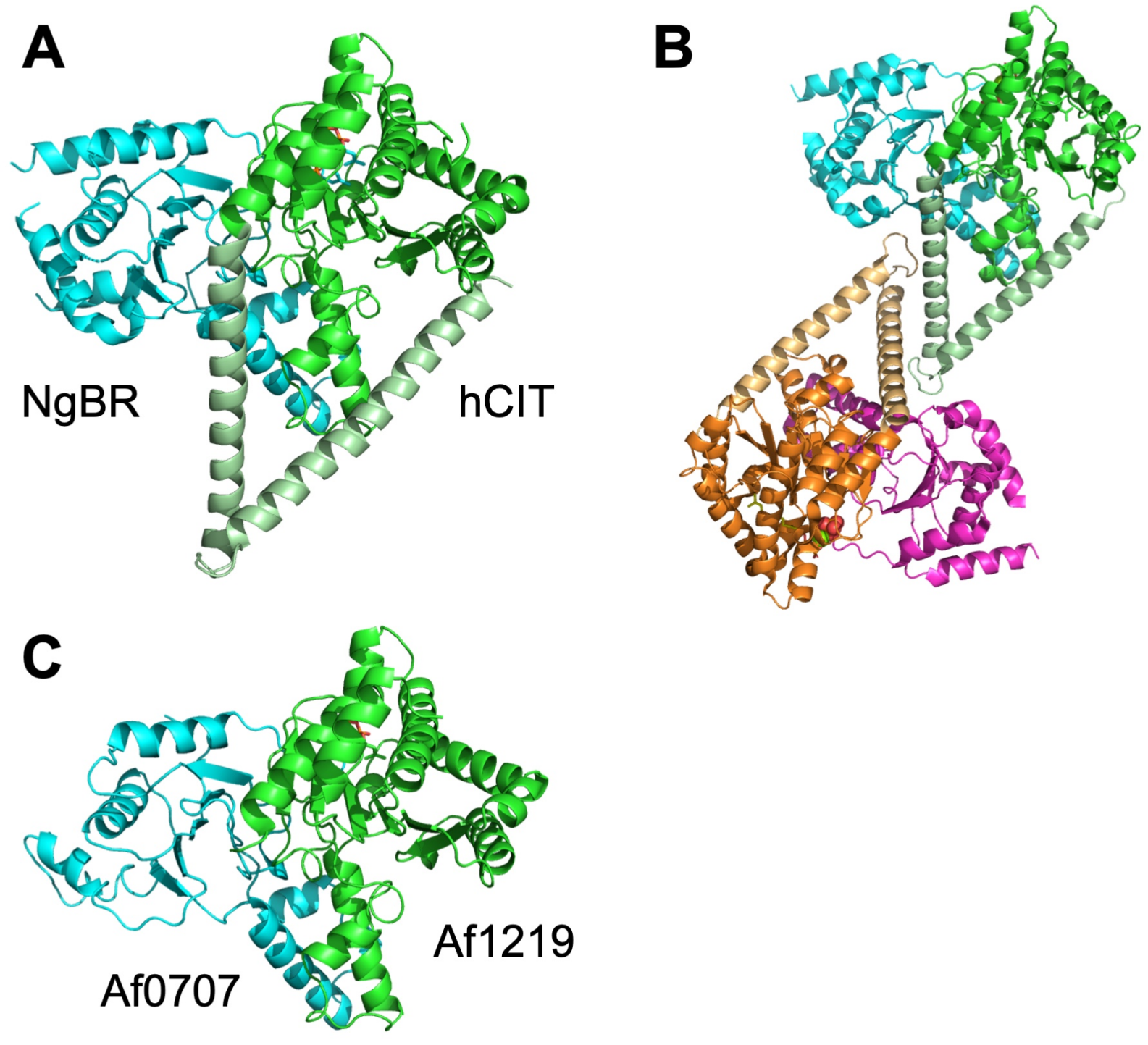
A
NgBR
hCIT
B
C
Af0707
Af1219